Precise measurement of weak strain by second-harmonic generation from silicon (111) surface

Ji-Hong Zhao,[1,*] Xian-Bin Li,[1] Zhan-Guo Chen,[1] Xing Meng,[2] and Gang Jia[1]

[1]*State Key Laboratory on Integrated Optoelectronics, College of Electronic Science and Engineering, Jilin University, 2699 Qianjin Street, Changchun 130012, China*
[2]*College of Physics, Jilin University, 119 Jiefang Road, Changchun 130012, China*
**Corresponding author: zhaojihong@jlu.edu.cn*

Received December 6, 2012; revised February 22, 2013; accepted March 17, 2013; posted March 19, 2013 (Doc. ID 181284); published April 12, 2013

The weak strain induced by uniaxial strain device is calibrated by strain-induced second-harmonic generation (SISHG) from silicon (111) surface. Dependences of the strain-induced second-harmonic intensity on sample azimuth angle show that the strain leads to increase of SH intensity. The high consistency of the SH-measured strain and the applied strain indicates that weak strain can be accurately calibrated by SISHG. The small applied strain does not greatly affect the 3 m symmetry of silicon (111) surface, but enhances the SH intensity evidently. The bulk inversion symmetry of crystal silicon vanished under applying of uniaxial strain and this also has demonstrated by first-principles simulation. Furthermore, the theoretical relative variation of Si–Si bond length agrees exactly with the applied strain along [111] direction.

OCIS codes: 190.2620, 190.4350.

1. INTRODUCTION

In complementary metal-oxide semiconductor (CMOS) structures, scaling is becoming increasingly more difficult technically and as a result the cost is reaching the level at which alternative methods are being sought to enhance device performance. New materials and device architectures are being proposed. Advances in deposition of tensile-strained silicon, along with its improved electron and hole mobility, has spurred much work from a number of reputable research groups [1–6]. In addition, properties of micronano devices, such as MOS transistor, are sensitively affected by the intrinsic mechanical strain built in silicon/silicon dioxide interface, which determines the displacement of atoms, subsurface layer symmetry modification, charge redistribution, dioxide-traps charging, and defect formation [7–9]. So developing a strain-calibrated technique is necessary for systematically detecting the strain exist in MOS device.

Numerous diagnostic procedures have been employed in the past for strain characterization of semiconductor samples, the most pronounced example being the optical techniques. They are nondestructive and offer the possibility of *in situ* applications. Raman spectroscopy [10], a well-established experimental tool, is based on the detection of strain-induced phonon frequency shifts. Piezo-electroreflectance and piezo-photoreflectance spectroscopy, on the other hand, are applied to investigate the effect of strain on the electronic bands [11,12]. These methods can detect strains in the range of 10^{-3}, which, however, is not sufficient in many applications. Optical second-harmonic generation (SHG) as a high-sensitivity nonlinear optical method has been implemented for *in situ* characterizing silicon surface by resolving the tiny change of centrosymmetry of Si bulk materials [8,13]. In addition, SHG provided a much higher sensitivity and thus promised to be suitable for the detection of very small amounts of strain (10^{-5}–10^{-4}).

In our previous work the strain-induced second-harmonic generation (SISHG) in silicon surface has been investigated, and the qualitatively quadratic relation between SH intensity and external strain was described and determined [14–16]. But the strain was not determined quantitatively by SHG measurements. In this paper, strain was quantitatively determined by SISHG and crystal structure of strained silicon was determined by first-principles calculation in theory.

2. STRAIN DEVICE AND SISHG EXPERIMENTS

In order to cause strain to silicon wafer, the uniaxial strain device was designed first and the schematic diagram is shown in the inset of Fig. 1. This strain device consisted of a micrometer system and could move a sharp edge against the center of a stripe supported at its ends by a fixed cover with a hole [17]. For small deformations compared with the dimensions of the silicon stripe there is a neutral surface in the middle part of the stripe. In order to form uniaxial strain, a silicon (111) wafer of 0.5 mm thickness was cut into narrow stripes (32 mm × 4 mm, a length/width ratio larger than 8) along the $[1\bar{1}0]$ direction, and the uniaxial strain was induced in the silicon stripe by moving the sharp edge of the strain device along the [111] direction (that is z axis), shown in Fig. 1. The tension strain along $[1\bar{1}0]$ direction of the silicon stripe (that is x axis) depends on deformation $J(r)$ described by equation $J(r) = J_0(a - r)(2a^2 + 2ar - r^2)/2a^3$, where r is the distance from the center of the stripe, $2a$ is the length of the silicon stripe, J_0 is the deformation at center of the stripe. By using this equation, the maximum strain ε_0 at the stripe center is independent of the elasticity of materials and it can be calculated as $\varepsilon_{xx} = \varepsilon_0 = 3hJ_0/2a^2$. As for the rest

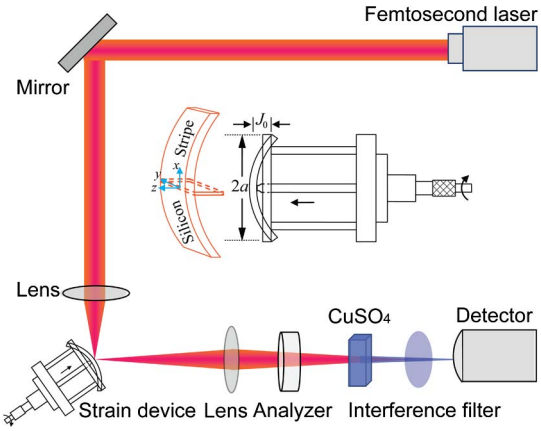

Fig. 1. (Color online) SHG experimental setup. The *s*-polarized fundamental light of 800 nm was focused onto the strained sample at an incident angle of 45° with respect to Si [111] direction. The reflected *p*-polarized and *s*-polarized SHG signal was selected using a polarimeter, filtered by the saturated $CuSO_4$ solution, and then detected by detector. Inset is a schematic diagram of uniaxial strain device.

of the strain components, only the one perpendicular to the surface of the stripe will be nonzero, and it can be calculated by the equation $\varepsilon_{zz} = \varepsilon_0[2(S_{11} + 2S_{12}) + (6S_{12} - S_{44})]/[8(S_{11} + 2S_{12}) + 2S_{44}]$, where S_{11}, S_{12}, and S_{44} are the elastic compliances of the material, for silicon the elastic compliances $S_{11} = 7.68 \times 10^{-12}$ Pa^{-1}, $S_{12} = -2.14 \times 10^{-12}$ Pa^{-1}, and $S_{44} = 12.56 \times 10^{-12}$ Pa^{-1}, so the strain along z axis can be calculated to $\varepsilon_{zz} = -0.356\varepsilon_{xx}$ [17,18].

By moving the sharp edge of the strain device, the center deformation of silicon stripe can be given from micrometer system and the strain value should be determined by equation $\varepsilon_{xx} = \varepsilon_0 = 3hJ_0/2a^2$ theoretically. Under the influence of a central force the stripe will develop along its long axis a strain proportional to the curvature. At the surface of a silicon stripe with thickness h this strain will be $\varepsilon_{xx} = \varepsilon_0 = h/2R$, R being the radius of curvature, which can be directly measured using the deflection of a laser beam [19]. The excellent fit of equation $\varepsilon_{xx} = \varepsilon_0 = h/2R$ to the data in [13] indicates that this strain device can be used for calculating the applied strain along the stripe without any adjustable parameters.

For SISHG measurement, the output of a femtosecond Ti-sapphire oscillator laser is used as a source of the fundamental radiation with the wavelength of 802 nm and the pulse width of 120 fs [16]. The experimental setup is similar as the SH-measured system described in [14], and the schematic diagram of this system is shown in Fig. 1. The incident light was focused onto the sample at an angle of 45° with respect to the z axis with *s*-polarization. The reflected light was selected by a polarization analyzer as *s*-polarization and *p*-polarization, respectively. Then the SH signal was filtrated orderly by the saturated $CuSO_4$ solution and a 400 nm interference filter, and finally detected by a detector that was composed of a photomultiplier tube and a lock-in amplifier. In SH experiments the strain device can rotate with revolving setup controlled by a step motor.

From the center deformation $J(r)$ expression of the strain device, it is obvious that the component of strain along x direction is inhomogeneous. An application of inhomogeneous strain to the silicon crystal can decrease its inversion symmetry [20]. So the inversion symmetry of silicon subsurface layer would be destroyed in the volume near the center of the strained silicon stripe. Therefore, in the dipole approximation, the bulk dipolar contribution in SH signals generated from silicon surface is not equal to zero. In other words, a strain-induced second-order nonlinear susceptibility appears and it will enhance the SH intensity evidently.

By rotating the silicon stripe around its surface normal to change the azimuthal angle, the *s*-in/*p*-out polarized and *s*-in/*s*-out polarized SH intensities as a function of the azimuthal angle of the silicon sample can be measured, respectively. According to the phenomenological theory, the *s*-in/*p*-out polarized and *s*-in/*s*-out polarized SH intensities generated from silicon surface can, respectively, be written as [10,20,21]

$$\begin{aligned} I_{s\to p}(2\omega) &= |a_{sp} + c_{sp}\cos 3\phi|^2 \\ &= \left[|a_{sp}|^2 + \frac{|c_{sp}|^2}{2}\right] + \mathrm{Re}(a_{sp}c_{sp}^*)[e^{i3\phi} + e^{-i3\phi}] \\ &\quad + \frac{|c_{sp}|^2}{4}[e^{i6\phi} + e^{-i6\phi}], \end{aligned} \tag{1}$$

$$I_{s\to s}(2\omega) = |b_{ss}\sin 3\phi|^2 = \frac{|b_{ss}|^2}{2} - \frac{|b_{ss}|^2}{4}[e^{i6\phi} + e^{-i6\phi}], \tag{2}$$

where azimuthal angle ϕ is measured from the $[1\bar{1}0]$ direction, for unstrained silicon $a_{s,p}$, $b_{s,s}$ and $c_{s,p}$ represent the total SH field strength which may result from the surface dipole, bulk quadrupole, and dc-electronic field-induced bulk dipole. Comparatively, for the strained silicon an additional strain-induced electric dipolar $\chi^{(2)}_{\mathrm{strain}}$ should be included in coefficients $a_{s,p}$, $b_{s,s}$, and $c_{s,p}$. As a result, for strained silicon both the *p*-polarized and *s*-polarized SH intensities should be increased compared with unstrained counterpart. The experimental results are in accord with our theoretical analysis very well and the experimental data are shown in Figs. 2(a) and 3(a), respectively. Curve A corresponds to the SH intensity generated from unstrained silicon surface and the SH signal of curve B is obtained from strained silicon with a strain value of $\varepsilon_0 = 3.86 \times 10^{-4}$. Compared to the SH intensity of Curve A and B at the same azimuthal angle, it is apparent that the application of strain can enhance the intensity of SH greatly. In a previous report [14], we considered that the external uniaxial strain can reduce the bulk inversion symmetry of silicon crystal, then such a small strain (about 10^{-4}) does not greatly affect the 3 m symmetry of silicon (111) surface, but it can enhance the SH intensity evidently. So the novanishing independent components of $\chi^{(2)}_{\mathrm{strain}}$ tensor still are $\chi^{(2),\mathrm{strain}}_{zzz}$, $\chi^{(2),\mathrm{strain}}_{zxx} = \chi^{(2),\mathrm{strain}}_{zyy}$, $\chi^{(2),\mathrm{strain}}_{yyy} = \chi^{(2),\mathrm{strain}}_{xxy}$. Also, this viewpoint would be provided by first-principles simulation.

3. RESULTS AND DISCUSSION

The *s*-in/*p*-out polarized SH electric field reflected from strained silicon is proportional to $\chi^{(2),\mathrm{strain}}_{zyy}$ [10,20], that is,

$$E_{s\to p}(2\omega) \propto i\chi^{(2),\mathrm{strain}}_{zyy} + K_{2z}(2\omega)\chi^{P}_{zyzy}, \tag{3}$$

where χ^{P}_{zyzy} is the bulk quadrupole contribution that is independent of the external strain, it is a constant containing the Fresnel reflection factors and $K_{2z}(2\omega)\chi^{P}_{zyzy} = 4 \times 10^{-10}$, $\chi^{(2),\mathrm{strain}}_{zyy}$ is the strain-induced component of second-order bulk contribution and it can be calculated as follows [14]:

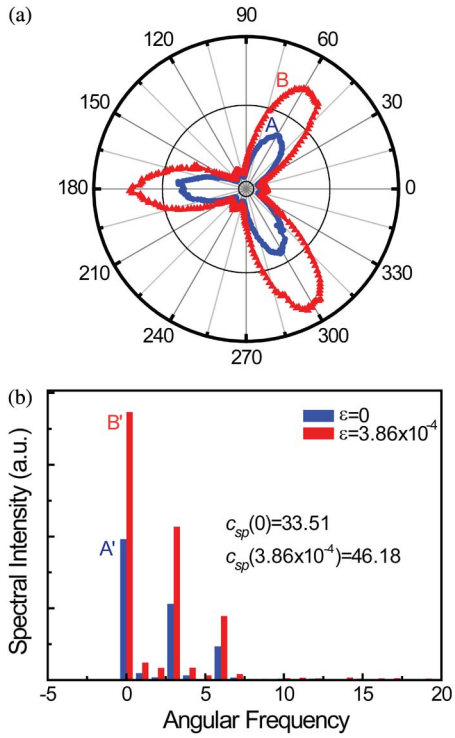

Fig. 2. (Color online) (a) *s*-polarized input/*p*-polarized output SH intensity as a function of azimuthal angle of Si (111) sample. Curve A corresponds to the SHG from unstrained Si (111) wafer and curve B is measured when the tensile strain is equal to 3.86×10^{-4}. (b) Fourier transforms of SHG patterns of (a). Graph A′ is the Fourier transform corresponding to curve A of (a) and graph B′ is the Fourier transform corresponding to curve B of (a).

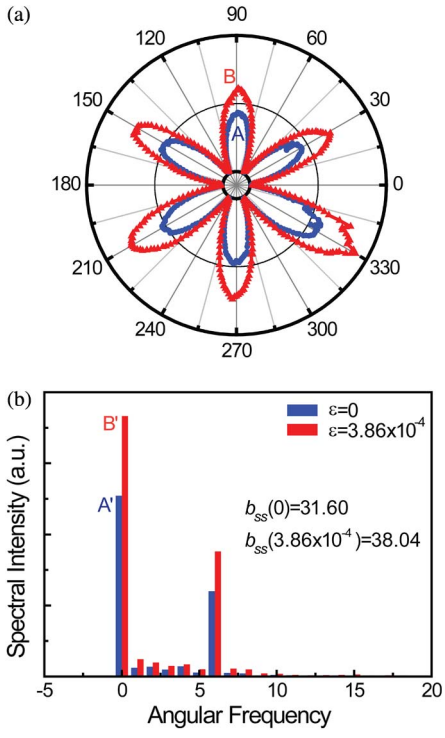

Fig. 3. (Color online) (a) *s*-polarized input/*s*-polarized output SH intensity as a function of azimuthal angle of Si (111) sample. Curve A corresponds to the SHG from unstrained Si (111) wafer and curve B is measured when the tensile strain is equal to 3.86×10^{-4}. (b) Fourier transforms of SHG patterns of (a). Graph A′ is the Fourier transform corresponding to curve A of (a) and graph B′ is the Fourier transform corresponding to curve B of (a).

$$\chi_{zyy}^{(2),\mathrm{strain}}(\mathrm{esu}) = 1.03 \times 10^{-6}\varepsilon_0. \tag{4}$$

According to its relation with $\chi_{zyy}^{(2),\mathrm{strain}}$, the other component $\chi_{yyy}^{(2),\mathrm{strain}}$ can be described as follows:

$$\chi_{yyy}^{(2),\mathrm{strain}}(\mathrm{esu}) = -0.78 \times 10^{-6}\varepsilon_0. \tag{5}$$

Figures 2(b) and 3(b) show the Fourier transform pattern of Figs. 2(a) and 3(a). From Fourier transformation spectrum of SH intensity, it is obvious that the fundamental, threefold, and sixfold frequency components are dominant for *s*-in/*p*-out polarized SHG; then for *s*-in-/*s*-out polarized SHG the fundamental and sixfold frequency components are dominant. The coefficients c_{sp} in Eq. (1) can be calculated by the Fourier transform. By using Eq. (3) we found that [10]

$$\frac{|c_{sp}(\mathrm{strain})|^2}{|c_{sp}(0)|^2} = \frac{|i\chi_{zyy}^{(2),\mathrm{strain}} + K_{2z}\chi_{zyzy}^{P}|^2}{|K_{2z}\chi_{zyzy}^{P}|^2} = 1 + \left|\frac{\chi_{zyy}^{(2),\mathrm{strain}}}{K_{2z}\chi_{zyzy}^{P}}\right|^2. \tag{6}$$

Here, $c_{sp}(\mathrm{strain})$ corresponds to the SH field strength from silicon (111) surface while external strain was applied to the silicon stripe, and $c_{sp}(0)$ corresponds to the SH field strength from unstrained silicon (111) surface. From the Fourier transform in Fig. 2(b), for the strain $\varepsilon_0 = 3.86 \times 10^{-4}$ calculated by deformation of the strain device, $c_{sp}(\mathrm{strain})/c_{sp}(0) = 1.380$. So the strain value obtained by the SH method can be calculated to $\varepsilon_0 = 3.69 \times 10^{-4}$ by Eq. (4).

Similarly, the strain value also can be obtained by $b_{ss}(\mathrm{strain})/b_{ss}(0)$ and Eq. (5). Replacing c_{sp} and $\chi_{\zeta yy}$ by b_{ss} and χ_{yyy}, respectively, the strain value can be calculated also by $b_{ss}(\mathrm{strain})/b_{ss}(0)$ with Eq. (6) From the Fourier transform in Fig. 3(b), for the strain $\varepsilon_0 = 3.86 \times 10^{-4}$ calculated by deformation of the strain device, $b_{ss}(\mathrm{strain})/b_{ss}(0) = 1.204$. So the strain value obtained by the SH method can be calculated to $\varepsilon_0 = 3.44 \times 10^{-4}$ by Eq. (5) and (6).

From the calculations we can find that the strain measured by SHG is very close to the value provided by the strain device and this is appreciate both for *s*-in/*p*-out and *s*-in/*s*-out polarized SH signal measurement. In other words, the strain formed in silicon stripe can be measured accurately by the SISHG method. For the difference between strain values "calculated by deformation of the strain device" and "obtained by the SH method," it is mainly caused by the accuracy of the strain device itself and the SH measurement system. Also the strain difference measured by SH between *p*-polarized and *s*-polarized SH mainly comes from the SH measurement system that would affect the accuracy of Fourier transformation coefficient evidently. From both the threefold symmetry in Fig. 2(a) and sixfold symmetry in Fig. 3(a) of SH intensity as a function of azimuthal angle we considered that the symmetry of strained silicon subsurface is similar to the symmetry of silicon (111) surface.

In this paper, we used first-principles simulation to describe the change of crystal structure after applying strain. For the uniaxial strain, the strain tensor can be expressed as

$$\varepsilon = \begin{pmatrix} \varepsilon_{xx} & 0 & 0 \\ 0 & 0 & 0 \\ 0 & 0 & \varepsilon_{zz} \end{pmatrix}. \tag{7}$$

In experiments, the strain of $\varepsilon_{xx} = 3.86 \times 10^{-4}$ is considered, the other two strain components are $\varepsilon_{yy} = 0$ and $\varepsilon_{zz} = -1.37 \times 10^{-4}$, respectively. Here, x, y, and z axis correspond to laboratorial coordinates: $[1\bar{1}0]$, $[11\bar{2}]$, and [111] crystallographic orientation, respectively. The strain tensor ε in crystallophysical coordinates by transformation of coordinates has the form

$$\begin{pmatrix} \varepsilon_{x'x'} \\ \varepsilon_{y'y'} \\ \varepsilon_{z'z'} \\ \varepsilon_{y'z'} \\ \varepsilon_{z'x'} \\ \varepsilon_{x'y'} \end{pmatrix} = \begin{pmatrix} (3\varepsilon_{xx} + 2\varepsilon_{zz})/6 \\ (3\varepsilon_{xx} + 2\varepsilon_{zz})/6 \\ \varepsilon_{zz}/3 \\ \varepsilon_{zz}/3 \\ \varepsilon_{zz}/3 \\ (-3\varepsilon_{xx} + 2\varepsilon_{zz})/6 \end{pmatrix} = \begin{pmatrix} 1.472 \times 10^{-4} \\ 1.472 \times 10^{-4} \\ -0.458 \times 10^{-4} \\ -0.458 \times 10^{-4} \\ -0.458 \times 10^{-4} \\ -2.388 \times 10^{-4} \end{pmatrix}, \quad (8)$$

where x', y', and z' are crystallophysical coordinates, they correspond to [100], [010], and [001] directions, respectively. So the stress tensor can be calculated with expression $\varepsilon_{ij} = S_{ijkl}\sigma_{kl}$, and they are

$$\sigma = \begin{pmatrix} \sigma_{x'x'} \\ \sigma_{y'y'} \\ \sigma_{z'z'} \\ \sigma_{y'z'} \\ \sigma_{z'x'} \\ \sigma_{x'y'} \end{pmatrix} = \begin{pmatrix} 0.03092 \\ 0.03092 \\ 0.01127 \\ -0.00365 \\ -0.00365 \\ -0.01901 \end{pmatrix} \text{(GPa)}. \quad (9)$$

Using the stress tensor mentioned above we simulated the crystal structure at the center of the strained silicon stripe using first-principles calculation. Our calculations were carried out using density-functional theory with a plane-wave basis set as implemented in the CASTEP code [22]. The core electrons are treated with Vanderbilt ultrasoft pseudopotentials [23]. All calculations are done with a cutoff energy of 160 eV. Lattice parameters of strained silicon and unstrained silicon crystal are marked in Table 1. The calculation results show that for crystal silicon lattice parameters $a = b = c$, $\alpha = \beta = \gamma = 90°$ that belong to cubic crystal system, then for the strained silicon lattice parameters $a = b \neq c$, $\alpha = \beta \neq \gamma \neq 90°$, so the silicon crystal symmetry was reduced and strain induced diapering of crystal silicon inversion symmetrical center. Figure 4 shows variation of Si–Si bond length of the crystal silicon before and after strain. Comparing Figs. 4(a) and 4(b), we find that all the four bond lengths of crystal silicon shorten under applying strain. In addition, the primary four equivalent Si–Si bond lengths of crystal silicon changed unequal after strain applying. Although the variation of Si–Si bond length is very small, it can reduce the inversion symmetry of crystal silicon remarkably and induce the second-order nonlinear effects. It is worth noting that the maximum of relative variation of Si–Si bond length is equal to 1.3694×10^{-4} according to Fig. 4. This value is very close to the

Table 1. Lattice Parameters Corresponding to Unstrained and Strained Silicon Crystal Structure, Respectively[a]

Lattice Parameters	a(Å)	b(Å)	c(Å)	α(°)	β(°)	γ(°)
Unstrained Si	5.39649	5.39649	5.39649	90.000	90.000	90.000
Strained Si	5.39587	5.39587	5.39631	89.998	89.998	89.991

[a]Coordinate axes of crystallophysical coordinates are [100], [010], and [001].

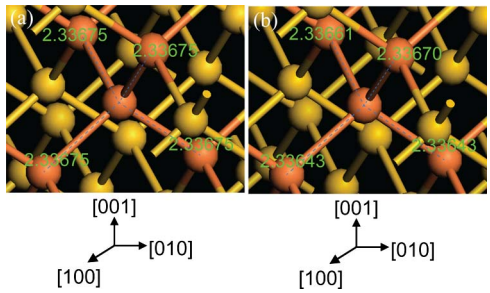

Fig. 4. (Color online) (a) Silicon crystal structure without external strain. (b) Silicon crystal structure with the existence of strain of $\varepsilon_{zz} = -1.37 \times 10^{-4}$.

applying strain value (1.37×10^{-4}) along [111] direction in experiment. It is different from experimental measurement results, first-principles simulation method can give a precise structure-parameter of silicon semiconductor from the atomic scale before and after straining. So the strain obtained from first-principles simulation is close to the known one. As a result, we can have a conclusion, for the small strain (10^{-4}), it can reduce the bulk symmetry of crystal silicon, but does not greatly affect the 3 m symmetry of silicon (111) surface.

4. CONCLUSION

In conclusion, the SISHG was investigated using the uniaxial strain device designed. The strain calculated by the SHG method agrees with that measured by the strain device very well both for *p*-polarized and *s*-polarized SH signal. First-principles calculations show that the external uniaxial strain can reduce the bulk inversion symmetry of crystal silicon due to change of crystal structure. Additionally, after strain applying the relative variation of Si–Si bond length agrees with the strain value along [111] direction very well. So this investigation gave direct evidence that SHG is a precise measurement method for small strain of semiconductor silicon surface.

ACKNOWLEDGMENTS

This work was funded by the NSFC (No. 11104109), the TNList cross-discipline foundation. This work was also partially supported by the National High-technology Research and Development Program of China (No. 2009AA03Z419), and NSFC (No. 61077026).

REFERENCES

1. Z. Kovats, T. Salditt, T. H. Metzger, J. Peisl, T. Stimpel, H. Lorenz, J. O. Chu, and K. Ismail, "Interface morphology in strained layer epitaxy of $Si/Si_{1-x}Ge_x$ layers studied by x-ray scattering under grazing incidence and atomic force microscopy," J. Phys. D **32**, 359–368 (1999).
2. H. M. Nayfeh, J. L. Hoyt, and D. A. Antoniadis, "Investigation of scaling methodology for strained Si *n*-MOSFETs using a calibrated transport model," in *2003 IEEE International Electron Devices Meeting*, Technical Digest (IEEE, 2003), pp. 475–478.
3. I. Aberg, O. O. Olubuyide, C. N. Chleirigh, I. Lauer, D. A. Antoniadis, J. Li, R. Hull, and J. L. Hoyt, "Electron and hole mobility enhancements in sub-10 nm-thick strained silicon directly on insulator fabricated by a bond and etch-back technique," in *2004 Symposium on Vlsi Technology*, Digest of Technical Papers (IEEE, 2004), pp. 52–53.
4. I. Aberg, O. O. Olubuyide, J. Li, R. Hull, and J. L. Hoyt, "Fabrication of strained Si/strained SiGe/strained si heterostructures on insulator by a bond and etch-back technique," in *Proceedings*

of the 2004 IEEE International Soi Conference (IEEE, 2004), pp. 35–36.
5. M. Casalino, L. Sirleto, L. Moretti, M. Gioffre, G. Coppola, and I. Rendina, "Silicon resonant cavity enhanced photodetector based on the internal photoemission effect at 1.55 μm: fabrication and characterization," Appl. Phys. Lett. **92**, 251104 (2008).
6. R. E. Belford, "Uniaxial tensile-strained Si devices," J. Electron. Mater. **30**, 807–811 (2001).
7. G. Lüpke, D. J. Bottomley, and H. M. van Driel, "SiO_2/Si interfacial structure on vicinal Si (100) studied with second-harmonic generation," Phys. Rev. B **47**, 10389–10394 (1993).
8. W. Daum, H. J. Krause, U. Reichel, and H. Ibach, "Identification of strained silicon layers at Si-SiO_2 interfaces and clean Si surfaces by nonlinear optical spectroscopy," Phys. Rev. Lett. **71**, 1234–1237 (1993).
9. H. Ibach, "The role of surface stress in reconstruction, epitaxial growth and stabilization of mesoscopic structures," Surf. Sci. Rep. **35**, 71–73 (1999).
10. J. Y. Huang, "Probing inhomogeneous lattice deformation at interface of Si(111)/SiO_2 by optical second-harmonic reflection and Raman spectroscopy," Jpn. J. Appl. Phys. **33**, 3878–3886 (1994).
11. F. H. Pollak and M. Cardona, "Piezo-electroreflectance in Ge, GaAs, and Si," Phys. Rev. **172**, 816–837 (1968).
12. B. C. Larson, C. W. White, T. S. Noggle, and D. Mills, "Synchrotron x-ray diffraction study of silicon during pulsed-laser annealing," Phys. Rev. Lett. **48**, 337–340 (1982).
13. C. W. van Hasselt, M. A. Verheijen, and T. Rasing, "Vicinal Si (111) surfaces studied by optical second-harmonic generation: step-induced anisotropy and surface-bulk discrimination," Phys. Rev. B **42**, 9263–9266 (1990).
14. J. H. Zhao, Q. D. Chen, Z. G. Chen, G. Jia, W. Su, Y. Jiang, Z. X. Yan, T. V. Dolgova, O. A. Aktsipetrov, and H. B. Sun, "Enhancement of second-harmonic generation from silicon stripes under external cylindrical strain," Opt. Lett. **34**, 3340–3342 (2009).
15. J. H. Zhao, B. W. Cheng, Q. D. Chen, W. Su, Y. Jiang, Z. G. Chen, G. Jia, and H. B. Sun, "Near-infrared femtosecond laser for studying the strain in $Si_{1-x}Ge_x$ alloy films via second-harmonic generation," IEEE Photon. J. **2**, 974–980 (2010).
16. J. H. Zhao, W. Su, Q. D. Chen, Y. Jiang, Z. G. Chen, G. Jia, and H. B. Sun, "Strain at native SiO_2/Si(111) interface characterized by strain-scanning second-harmonic generation," IEEE J. Quantum Electron. **47**, 55–59 (2011).
17. E. Liarokapis, D. Papadimitriou, J. Rumberg, and W. Richter, "Raman and RAS measurements on uniaxially strained thin semiconductor layers," Phys. Status Solidi B **211**, 309–316 (1999).
18. D. Papadimitriou and W. Richter, "Highly sensitive strain detection in silicon by reflectance anisotropy spectroscopy," Phys. Rev. B **72**, 075212 (2005).
19. E. Liarokapis and W. Richter, "Design of two devices for biaxial stresses and their application to silicon wafers," Meas. Sci. Technol. **3**, 347–351 (1992).
20. S. V. Govorkov, V. I. Emel'yanov, N. I. Koroteev, G. I. Petrov, I. L. Shumay, and V. V. Yakovlev, "Inhomogeneous deformation of silicon surface layers probed by second-harmonic generation in reflection," J. Opt. Soc. Am. B **6**, 1117–1124 (1989).
21. J. E. Sipe, D. J. Moss, and H. M. van Driel, "Phenomenological theory of optical second- and third-harmonic generation from cubic centrosymmetric crystals," Phys. Rev. B **35**, 1129–1141 (1987).
22. M. D. Segall, Philip J. D. Lindan, M. J. Probert, C. J. Pickard, P. J. Hasnip, S. J. Clark, and M. C. Payne, "First-principles simulation: ideas, illustrations and the CASTEP code," J. Phys. Condens. Matter **14**, 2717–2744 (2002).
23. D. Vanderbilt, "Soft self-consistent pseudopotentials in a generalized eigenvalue formalism," Phys. Rev. B **41**, 7892–7895 (1990).